

# Quantifying Efficiency Loss of Perovskite Solar Cells by a Modified Detailed Balance Model

Wei E. I. Sha, Hong Zhang, Zi Shuai Wang, Hugh L. Zhu, Xingang Ren, Francis Lin, Alex K.-Y. Jen, and Wallace C. H. Choy\*

A modified detailed balance model is built to understand and quantify efficiency loss of perovskite solar cells. The modified model captures the light-absorption-dependent short-circuit current, contact and transport-layer-modified carrier transport, as well as recombination and photon-recycling-influenced open-circuit voltage. The theoretical and experimental results show that for experimentally optimized perovskite solar cells with the power conversion efficiency of 19%, optical loss of 25%, nonradiative recombination loss of 35%, and ohmic loss of 35% are the three dominant loss factors for approaching the 31% efficiency limit of perovskite solar cells. It is also found that the optical loss climbs up to 40% for a thin-active-layer design. Moreover, a misconfigured transport layer introduces above 15% of energy loss. Finally, the perovskite-interface-induced surface recombination, ohmic loss, and current leakage should be further reduced to upgrade device efficiency and eliminate hysteresis effect. This work contributes to fundamental understanding of device physics of perovskite solar cells. The developed model offers a systematic design and analysis tool to photovoltaic science and technology.

mechanism and quantify the efficiency loss for perovskite solar cells.

The analysis and quantification of efficiency loss of solar cells can be done by the drift-diffusion model,<sup>[24,25]</sup> circuit model,<sup>[26,27]</sup> and detailed balance model.<sup>[28,29]</sup> Due to a high nonlinearity of coupled equations and a complex device configuration, drift-diffusion model is difficult to retrieve simulation parameters from the measured current density–voltage ( $J$ – $V$ ) curves. The parameters include recombination rate, mobility, energy levels (e.g., conduction band, valence band, and work function), effective density of states, and injection/extraction barrier heights. Furthermore, the drift-diffusion model is nontrivial to describe the photon recycling effect correctly.<sup>[30]</sup> Concerning the circuit model, it requires to retrieve five parameters in modeling. Hence, the uniqueness of the parameters is questionable.

## 1. Introduction


Due to merits of direct bandgap,<sup>[1–4]</sup> high and balanced carrier mobility,<sup>[5,6]</sup> long electron-hole diffusion length,<sup>[7–9]</sup> low non-radiative Auger recombination,<sup>[10]</sup> and high internal quantum efficiency,<sup>[11]</sup> perovskite solar cells show a great potential to be the next-generation high-performance photovoltaics. A great amount of schemes have been proposed to enhance device performances<sup>[12–22]</sup> and to promote power conversion efficiency (PCE) up to 22%.<sup>[23]</sup> However, limited works discuss the loss

Also, the ideality factor in the circuit model has ambiguous physical meaning and cannot quantitatively represent radiative recombination (photon recycling) and nonradiative (Auger and Shockley-Read-Hall) recombination separately. Additionally, while the traditional detailed balance model demonstrates a strong capability to predict the efficiency limit of an ideal solar cell, the model cannot quantify the energy loss of a practical solar cell including optical and electrical (thermodynamic) loss. In this work, a revised detailed balance model is proposed to unveil the loss mechanism and quantify the loss factors of perovskite solar cells. Through investigating the device performance of various fabricated perovskite solar cells, the three dominant loss factors of optical loss, nonradiative recombination loss, and ohmic loss are identified quantitatively. The perovskite-interface-induced surface recombination, ohmic loss, and current leakage are also analyzed. Consequently, the work offers a guideline to the researchers for optimizing perovskite solar cells and ultimately approaching the Shockley–Queisser limit of photovoltaics.<sup>[29]</sup>

Dr. W. E. I. Sha, H. Zhang, Z. S. Wang, Dr. H. L. Zhu, Dr. X. G. Ren, Prof. W. C. H. Choy  
Department of Electrical and Electronic Engineering  
The University of Hong Kong  
Pokfulam Road, Hong Kong, P. R. China  
E-mail: chchoy@eee.hku.hk

F. Lin, Prof. A. K.-Y. Jen  
Department of Materials Science & Engineering  
University of Washington  
Seattle, WA 98195, USA

Prof. A. K.-Y. Jen  
Department of Physics and Materials Science  
City University of Hong Kong  
Kowloon Tong, Hong Kong, P. R. China

 The ORCID identification number(s) for the author(s) of this article can be found under <https://doi.org/10.1002/aenm.201701586>.

DOI: 10.1002/aenm.201701586

## 2. Results and Discussion

### 2.1. Theory

In order to understand the loss mechanism and qualify loss factors, we propose the revised detailed balance model, which is expressed as

$$J = \frac{V - JR_s}{R_{sh}} + J_n(V - JR_s) + J_r(V - JR_s) - J_p \quad (1)$$

where  $V$  is the applied voltage of a solar cell.  $J_p$  is the photocurrent.  $J_r$  and  $J_n$  are the current loss due to the radiative emission by photon recycling and the nonradiative recombination by defects and impurities, respectively.  $R_s$  is the series resistance, which describes the ohmic loss by the contacts, carrier transport layers, and the heterojunction interfaces between the perovskite and carrier transport layers. The defects and voids-induced current leakage is represented by the shunt resistance  $R_{sh}$ .

The photocurrent is given by

$$J_p = q \int_0^\infty \alpha(\lambda, L) \frac{\Gamma(\lambda)\lambda}{hc_0} d\lambda \quad (2)$$

where  $c_0$  is the speed of light in air,  $\Gamma$  is the AM 1.5G spectrum of Sun,  $\lambda$  is the wavelength, and  $q$  is the elementary charge. The absorptivity  $\alpha$  is the ratio of power absorbed by the perovskite active layer over the power of incident sunlight, which depends on the thickness of the perovskite layer  $L$ , refractive indices of materials adopted, and light-trapping structures. It can be obtained by numerically solving Maxwell equation.<sup>[31]</sup>

The radiative current is written as

$$J_r(V - JR_s) = J_0^r \left[ \exp\left(\frac{q(V - JR_s)}{k_B T}\right) - 1 \right] \quad (3)$$

where  $k_B$  is the Boltzmann constant and  $T$  is the Kelvin temperature. Here, the radiative saturation current  $J_0^r$  is of the form<sup>[28]</sup>

$$J_0^r = q \int_0^\infty \alpha(\lambda, L) \frac{\Gamma_0(\lambda)\lambda}{hc_0} d\lambda \quad (4)$$

It is proportional to the spectral overlap integral between the absorptivity  $\alpha$  and black-body (thermal) emission spectrum  $\Gamma_0$  at room temperature ( $T = 300$  K).

For perovskite solar cells, the dominant nonradiative recombination is the Shockley-Read-Hall (defect-assisted) recombination.<sup>[32,33]</sup> Thus, the bulk nonradiative current reads

$$J_n(V - JR_s) = J_0^n \exp\left(\frac{q(V - JR_s)}{2k_B T}\right), \quad J_0^n = q\gamma n_i L \quad (5)$$

where  $\gamma$  is the nonradiative recombination rate depending on the crystalline quality of the perovskite film, and  $n_i$  is the intrinsic carrier density of bulk perovskite material. The Equation (5) can also be used to describe the surface nonradiative current if one replaces  $n_i L$  by an equivalent surface intrinsic carrier density.

The modified detailed balance model is different from existing solar cell models (see Note 1S in the Supporting Information) in literature. First, it is much simpler than the drift-diffusion model and considers the photon recycling effect. Second, compared with the circuit model, in the revised detailed balance model, the radiative saturation current is not an unknown parameter needed to be retrieved from experimental data. The radiative saturation current can be calculated with Maxwell's equations and black-body radiation law. Meanwhile, the nonradiative recombination is fully considered in the modified model. Contrarily, it is implicit and inaccurate in the circuit model, which is expressed as the ideality factor.

With the proposed model, (1) we can capture optical effects including light trapping and angular restriction in terms of the absorptivity  $\alpha$  and thermal emission spectrum  $\Gamma_0$  of perovskite cells. (2) We can describe complete recombination mechanisms including radiative and nonradiative recombination. (3) We can investigate the influences of carrier transport layers and contacts on the electrical response of perovskite solar cells. (4) We can quantify the loss factors in perovskite solar cells involving optical loss, recombination loss, ohmic loss (by series resistance), and current leakage loss (by shunt resistance).

Given a  $J$ - $V$  curve, our model will adopt the nonlinear Newton's method<sup>[34]</sup> to retrieve only the three parameters including the nonradiative recombination rate  $\gamma$ , the series resistance  $R_s$ , and the shunt resistance  $R_{sh}$ . The intrinsic carrier density of  $\text{CH}_3\text{NH}_3\text{PbI}_3$  (MAPbI<sub>3</sub>) material is  $10^9 \text{ cm}^{-3}$ .<sup>[5]</sup> The refractive index of the MAPbI<sub>3</sub> material is obtained by the Forouhi-Bloomer model, which is in well agreement with experimental results measured via other methods such as ellipsometry.<sup>[35]</sup>

## 2.2. Analysis of Experiment Results

Figure 1 shows the investigated device structure and corresponding energy diagram. The fabrication methods are described in the Experimental Section.  $\text{NiO}_x$  and PEDOT:PSS are the hole transport layers (HTL).  $\text{C}_{60}$  is the electron transport layer (ETL). Bis- $\text{C}_{60}$  and zirconium acetylacetonate ( $\text{ZrAcAc}$ ) are employed as the electron-selective interfacial layers at the

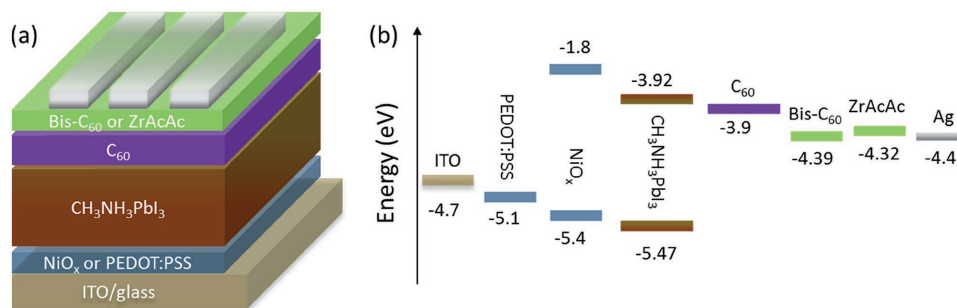


**Figure 1.** a) Device structure of perovskite solar cells and b) corresponding energy band diagram.

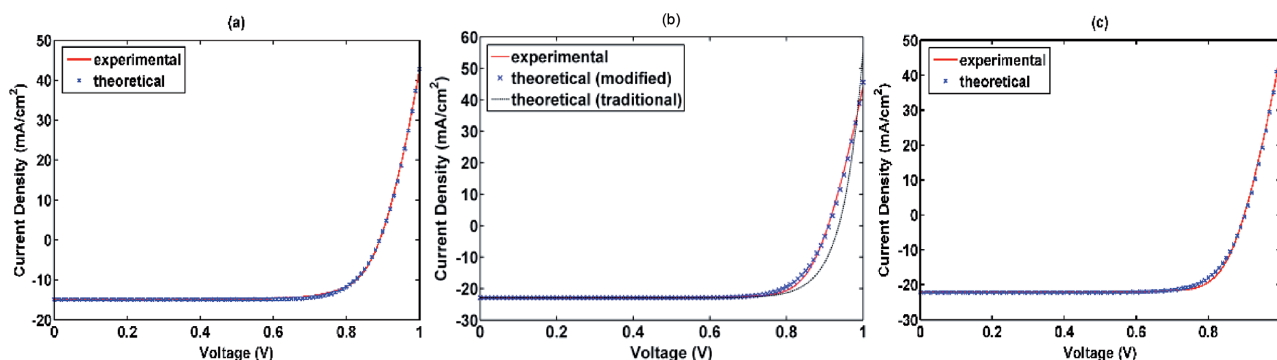


**Figure 2.** The theoretical and experimental  $J$ - $V$  characteristics of perovskite solar cells with different active layer thickness. a) 80 nm, b) 200 nm, c) 240 nm. The relative fitting errors for the three cases are respectively a) 1.44%, b) 2.41%, and c) 2.40%. All the  $J$ - $V$  characteristics are fitted by the modified detailed balance model. For a comparative study, b) also presents the result fitted by the traditional detailed balance model.

organic/cathode interface.<sup>[14]</sup> ITO and Ag layers are the anode and cathode, respectively. The MAPbI<sub>3</sub> perovskite films are fabricated by a modified antisolvent method.<sup>[14]</sup>

### 2.2.1. Active Layer Thickness

The device structures of MAPbI<sub>3</sub> perovskite solar cells with different active layer thickness are given as follows:

ITO/NiO<sub>x</sub> (20 nm)/MAPbI<sub>3</sub> (80 nm)/C<sub>60</sub> (50 nm)/Bis-C<sub>60</sub> (10 nm)/Ag (120 nm)  
ITO/NiO<sub>x</sub> (20 nm)/MAPbI<sub>3</sub> (200 nm)/C<sub>60</sub> (50 nm)/Bis-C<sub>60</sub> (10 nm)/Ag (120 nm)  
ITO/NiO<sub>x</sub> (20 nm)/MAPbI<sub>3</sub> (240 nm)/C<sub>60</sub> (50 nm)/Bis-C<sub>60</sub> (10 nm)/Ag (120 nm)

**Figure 2** depicts the theoretically fitted and experimentally measured  $J$ - $V$  curves (with the reverse scanning). The relative fitting error is around 2% for all the cases, which suggests that the modified detailed balance model well captures the device physics of perovskite solar cells. However, the traditional detailed balance model that does not incorporate the series and shunt resistances produces noticeable errors as illustrated in **Figure 2b**.

**Table 1** lists the retrieved characteristic parameters from the measured  $J$ - $V$  curves. **Figure 3** shows the quantitative efficiency loss for the perovskite cells with reference to the Shockley–Queisser limit, i.e., short-circuit current ( $J_{sc}$ ) of 25.88 mA cm<sup>-2</sup>, open-circuit voltage ( $V_{oc}$ ) of 1.31 V, fill factor (FF) of 0.91, and PCE of 30.75%. For achieving the Shockley–Queisser limit, the nonradiative recombination should be

ignorable ( $\gamma = 0$ ). Meanwhile, the series resistance is zero ( $R_s = 0$ ) and the shunt resistance goes to infinity ( $R_{sh} \rightarrow \infty$ ). After carefully studying **Table 1** and **Figure 3**, we can understand the evolution of the loss factors as the thickness of active layer increases.

- (1) Since thin perovskite active layer (e.g., 80 nm) has a weak optical absorption, optical loss is a dominant loss factor and thus a low  $J_{sc}$  value is obtained. The low  $J_{sc}$  reduces the  $V_{oc}$ , FF, and PCE.<sup>[28,30]</sup> In **Table 1**, the thin perovskite layer exhibits the largest nonradiative recombination rate  $\gamma$  owing to the low-quality film formation (with low crystallinity and many grain boundaries)<sup>[36]</sup> resulting in a significant hysteresis effect (see **Figure S1**, Supporting Information). However, the thin-active-layer configuration achieves the smallest nonradiative recombination current (loss) that is proportional to the product of the recombination rate  $\gamma$  and the active layer thickness  $L$ , as presented in Equation (5). As the thickness  $L$  increases, the nonradiative recombination loss increases, although the corresponding recombination rate decreases and no hysteresis effect can be observed (see **Figure S1**, Supporting Information). Regarding the thicker perovskite layer, the optical loss is still large (around 40%) for the device configuration achieving the maximum PCE. Hence, both light-trapping design and formation of high-quality thicker perovskite film are critically important to boost device performance of perovskite photovoltaics.
- (2) Because of well-engineered designs of both electron and HTL, the loss by shunt current can be ignored (with

**Table 1.** The retrieved characteristic parameters from measured  $J$ - $V$  curves of perovskite solar cells with different active layer thickness.  $L$  means thickness.  $\gamma$ ,  $R_s$ , and  $R_{sh}$  are the nonradiative recombination rate, series resistance, and shunt resistance. The loss of  $J_{sc}$ ,  $V_{oc}$ , and FF with respect to their Shockley–Queisser limiting values are also calculated.

$L$ [nm]	$\gamma$ [s <sup>-1</sup> ]	$R_s$ [10 <sup>-4</sup> Ohm m <sup>2</sup> ]	$R_{sh}$ [10 <sup>4</sup> Ohm m <sup>2</sup> ]	$J_{sc}$ [mA cm <sup>-2</sup> ]	$V_{oc}$ [V]	FF	PCE [%]
80	543	0.91	0.77	14.86/43%	0.89/32%	0.75/18%	9.92
200	228	0.71	0.85	22.97/11%	0.91/31%	0.80/12%	16.72
240	219	0.83	0.57	22.11/14%	0.90/31%	0.80/12%	15.92

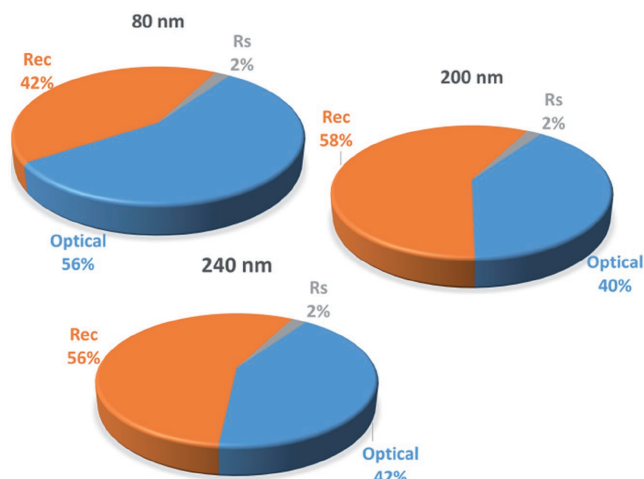


**Figure 3.** Efficiency loss of  $\text{CH}_3\text{NH}_3\text{PbI}_3$  solar cells with the active layer thickness of 80, 200, and 240 nm.

sufficiently large shunt resistances) and the ohmic loss (with small series resistances) is as below as 2%. On the one hand, thin perovskite film yields a low photocurrent due to the optical loss. On the other hand, it is clear that thick perovskite film absorbs more light and thus produces a larger photocurrent, while too-thick thickness causes loss of photovoltage, most likely due to the increased nonradiative recombination loss.

- (3) The nonradiative recombination loss is boosted when the thickness increases (see Figure 3). The increased nonradiative recombination is responsible for the reduction of  $V_{oc}$  and FF. Most importantly, the nonradiative recombination is the leading loss mechanism for the cell with the maximum PCE. Therefore, improving the crystallinity<sup>[12]</sup> and reducing the grain boundaries of thick perovskite films are critically important to fabricate highly efficient perovskite solar cells. Meanwhile, passivation of perovskite grain boundaries has also been demonstrated to effectively reduce the nonradiative recombination.<sup>[37]</sup>

### 2.2.2. Carrier Transport Layer

The  $\text{MAPbI}_3$  solar cells with different carrier transport layers are given as follows

ITO/ $\text{NiO}_x$  (20 nm)/ $\text{MAPbI}_3$  (200 nm)/ $\text{C}_{60}$  (50 nm)/Bis- $\text{C}_{60}$  (10 nm)/Ag (120 nm)  
 ITO/PEDOT:PSS (40 nm)/ $\text{MAPbI}_3$  (200 nm)/ $\text{C}_{60}$  (50 nm)/Bis- $\text{C}_{60}$  (10 nm)/Ag (120 nm)  
 ITO/ $\text{NiO}_x$  (20 nm)/ $\text{MAPbI}_3$  (200 nm)/ $\text{C}_{60}$  (50 nm)/ZrAcAc (10 nm)/Ag (120 nm)

In contrast to the optimized device structure where  $\text{NiO}_x$ ,  $\text{C}_{60}$ , and Bis- $\text{C}_{60}$  function as HTL, ETL, and electron selective interface layer, respectively, one case is to replace  $\text{NiO}_x$  by PEDOT:PSS and the other is to replace Bis- $\text{C}_{60}$  by ZrAcAc. Regarding the ZrAcAc case, the ZrAcAc layer is employed to modulate the interfacial properties of the cathode. Although Figure 4 shows the theoretically fitted and experimentally measured  $J$ - $V$  curves (with reverse scanning). Table 2 lists the retrieved characteristic parameters from the measured  $J$ - $V$  curves. Interestingly, the ZrAcAc case shows the maximum fitting error of 3.27%, which can be observed clearly in Figure 4b as compared with Figures 2 and 4a. The injection barrier with an abnormally large  $V_{oc}$  of 0.94 V (see Table 2) induced by the ZrAcAc layer makes the modified detailed balance model slightly inaccurate.

The quantitative energy loss for the perovskite cells with different carrier transport layers are illustrated in Figure 5. A drastically amplified ohmic loss and shunt current loss are clearly observed. The ohmic loss is around 6%. The current leakage loss even reaches 15% for the ZrAcAc case. The enlarged loss can be understood by the increased series resistance and pronouncedly decreased shunt resistance as listed in Table 2. Therefore, an improper design of carrier transport layer will introduce significant loss channels by additional resistances and significantly lower the FF. Moreover, the  $J_{sc}$  reduction of the PEDOT:PSS case is caused by a larger optical reflectance. It is because that PEDOT:PSS has a larger refractive index than  $\text{NiO}_x$ . The reduced  $J_{sc}$  will also diminish  $V_{oc}$ . Additionally, no matter which transport layer is adopted, the optical loss fraction

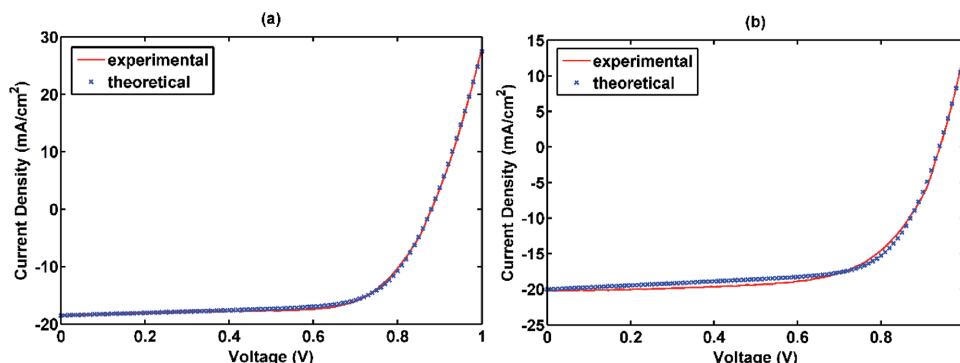


**Figure 4.** The theoretical and experimental  $J$ - $V$  characteristics for perovskite solar cells incorporating different carrier transport layers. a) PEDOT:PSS and Bis- $\text{C}_{60}$  are the HTL and electron selective interfacial layer, respectively. b)  $\text{NiO}_x$  and ZrAcAc are the HTL and electron selective interfacial layer, respectively. The relative fitting errors for the two cases are respectively a) 1.57%, b) 3.27%. All the  $J$ - $V$  characteristics are fitted by the modified detailed balance model.

**Table 2.** The retrieved characteristic parameters from measured  $J$ - $V$  curves of perovskite solar cells incorporating different carrier transport layers. The loss of  $J_{sc}$ ,  $V_{oc}$ , and FF with respect to their Shockley–Queisser limiting values are also calculated.

HTL/interfacial layer	$\gamma$ [s <sup>-1</sup> ]	$R_s$ [10 <sup>-4</sup> Ohm m <sup>2</sup> ]	$R_{sh}$ [10 <sup>4</sup> Ohm m <sup>2</sup> ]	$J_{sc}$ [mA cm <sup>-2</sup> ]	$V_{oc}$ [V]	FF	PCE [%]
NiO <sub>x</sub> /Bis-C <sub>60</sub>	228	0.71	0.85	22.97/11%	0.91/31%	0.80/12%	16.72
PEDOT/Bis-C <sub>60</sub>	299	2.53	4.32 × 10 <sup>-6</sup>	18.63/28%	0.88/33%	0.69/24%	11.31
NiO <sub>x</sub> /ZrAcAc	101	2.56	3.55 × 10 <sup>-6</sup>	20.14/22%	0.94/28%	0.66/27%	12.49

is almost unchanged, which is as high as 40% for the thin perovskite film configuration.

### 2.2.3. Overall Device Performances

Regarding hysteresis effect, we can compare the retrieved parameters for different scanning scenarios (see Table 3). The relative fitting errors are 3.34% and 1.57%, respectively, for the forward and reverse scanning cases (see Figure S2, Supporting Information and Figure 4a). The larger fitting error in the forward scanning indicates that there is an injection barrier, resulting in a larger  $V_{oc}$  as listed in Table 2. Simultaneous modifications of all the retrieved parameters ( $\gamma$ ,  $R_{sh}$ , and  $R_s$ ), together with the injection barrier, unveil a complicated mechanism of hysteresis at the interface between the MAPbI<sub>3</sub> and PEDOT:PSS layers. It is well known that ions in perovskite will be driven by the internal electrostatic field of the cell. The ions will migrate in the perovskite layer and accumulate at the interfaces between the perovskite and carrier transport layer (PEDOT:PSS) that blocks ions. The migration and accumulation of ions will in turn induce an inhomogeneous spatial distribution of the internal field, which significantly influences the carrier transport by introducing the injection barrier, modifying the surface recombination ( $\gamma$ ), and induce the surface ohmic loss and current leakage ( $R_s$  and  $R_{sh}$ ). The simultaneous evolution of all the characteristic parameters under different scanning directions is caused by a complex nonlinear coupling and

a giant mobility (relaxation time) difference between carrier transport and ion migration.

The modified detailed balance model is finally employed to quantify the energy loss of optimized and high-performance perovskite solar cells (see Figure 6). Figure S3 in the Supporting Information shows the corresponding experimental and theoretical results of  $J$ - $V$  characteristics, with a very small relative fitting error of 0.48%. Such a small error strongly indicates that the modified model near-perfectly captures the device physics of high-performance perovskite cells free from unwanted injection and extraction barriers. The total thermodynamic loss caused by series resistance, shunt resistance, and nonradiative recombination is 75%, in comparison with the optical loss of 25%. The reductions of  $J_{sc}$ ,  $V_{oc}$ , FF, and PCE with reference to the corresponding Shockley–Queisser limit are 12%, 16%, 15%, and 37%. In contrast to the  $J_{sc}$  loss, both the  $V_{oc}$  and FF losses are mainly from the perovskite interfaces. Thus, suppressing the interface loss by reducing series resistance and surface recombination is essential to upgrade the efficiency to approach the detailed balance limit.

## 3. Conclusion

We proposed a modified detailed balance model, which shows significant advantages to quantify and understand the efficiency loss of perovskite solar cells. Our experimental and theoretical results show that for thin-active-layer design, light trapping is needed to reduce the dominant optical loss. For optimum device structures, the well-engineered carrier transport layers and high-quality perovskite film are essential to reduce the dominant ohmic loss and defect/impurity-induced recombination loss. Our work offers a simple and reliable modeling methodology and insightful understanding to efficiency loss of perovskite solar cells. The model can serve as a general design tool to analyze other emerging solar cells.

## 4. Experimental Section

**Materials:** All the chemicals and materials were purchased and used as received unless otherwise noted. PEDOT:PSS (Baytron Al 4083) was purchased from H. C. Starck GmbH, Germany. CH<sub>3</sub>NH<sub>3</sub>I was purchased from Dyesol and used as received. PbI<sub>2</sub> (99%) was purchased from Sigma-Aldrich. Bis-C<sub>60</sub> surfactant was provided by Prof. Alex K.-Y. Jen's group. NiO<sub>x</sub> NCs inks were prepared according to our previous reports.<sup>[14,38]</sup>

**Device Fabrication:** ITO-coated glass substrates were cleaned and then ultraviolet–ozone treated for 20 min. PEDOT:PSS (Baytron Al 4083) was spin-coated with thickness of 45 nm and then dried at 150 °C for

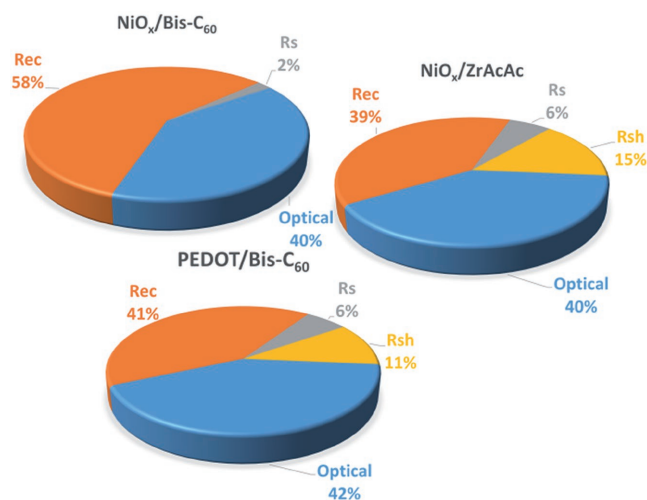


**Figure 5.** The dependence of efficiency loss of CH<sub>3</sub>NH<sub>3</sub>PbI<sub>3</sub> solar cells on the carrier transport layer configurations.



**Table 3.** The retrieved characteristic parameters from measured  $J$ - $V$  curves of perovskite solar cells with PEDOT:PSS and Bis-C<sub>60</sub> as hole transport and interfacial layers, respectively. The  $J$ - $V$  curves are measured with the reverse and forward scanning.

PEDOT:PSS/ Bis-C <sub>60</sub>	$\gamma$ [s <sup>-1</sup> ]	$R_s$ [10 <sup>-4</sup> Ohm m <sup>2</sup> ]	$R_{sh}$ [10 <sup>4</sup> Ohm m <sup>2</sup> ]	$J_{sc}$ [mA cm <sup>-2</sup> ]	$V_{oc}$ [V]	FF	PCE [%]
Forward	115	4.32	$3.47 \times 10^{-6}$	18.65	0.93	0.63	10.99
Reverse	299	2.53	$4.32 \times 10^{-6}$	18.63	0.88	0.69	11.31

10 min. The NiO<sub>x</sub> NCs ink (20 mg mL<sup>-1</sup> in DI water) was spin-coated to obtain 20 nm NiO<sub>x</sub> film. The resultant NiO<sub>x</sub> films would be used to fabricate devices without annealing process or other treatments. The 1 M CH<sub>3</sub>NH<sub>3</sub>PbI<sub>3</sub> solution was prepared by reacting the CH<sub>3</sub>NH<sub>3</sub>I powder and PbI<sub>2</sub> in  $\gamma$ -butyrolactone:dimethyl sulfoxide = 7: 3 (v/v) at 60 °C for 1 h. The perovskite precursor solution was deposited onto a NiO<sub>x</sub>/ITO or PEDOT:PSS/ITO substrate by a consecutive two-step spin-coating process at 1000 rpm and at 4000 rpm for 20 and 40 s, respectively, and 180  $\mu$ L of toluene was rapidly poured on top of the substrates during spin coating in the second spin stage which is slightly modified method from the reported protocol.<sup>[14]</sup> The obtained films were dried on a hot plate at 100 °C for 10 min. Perovskite layers with different thickness were obtained by varying the precursor concentration. Subsequently, the C<sub>60</sub> (20 mg mL<sup>-1</sup> in dichlorobenzene) and Bis-C<sub>60</sub> surfactant (2 mg mL<sup>-1</sup> in isopropyl alcohol) or Zirconium(IV) acetylacetonate (ZrAcAc) (2 mg mL<sup>-1</sup> in anhydrous ethanol) were then sequentially deposited by spin coating at 1000 rpm for 60 s and 3000 rpm for 40 s, respectively.

For the best-performance devices, the perovskite precursor was modified by Cl-doping approach. The CH<sub>3</sub>NH<sub>3</sub>I (190 mg) was mixed with PbI<sub>2</sub> (500 mg) and PbCl<sub>2</sub> (30 mg) in anhydrous *N,N*-dimethylformamide (1 mL) by shaking at room temperature for 20 min to produce a clear CH<sub>3</sub>NH<sub>3</sub>PbI<sub>3</sub>(Cl) solution. To deposit perovskite film, the CH<sub>3</sub>NH<sub>3</sub>PbI<sub>3</sub>(Cl) solution was first dropped onto a NiO<sub>x</sub>/ITO substrate. The substrate was then spun at 5000 rpm and after 6 s, anhydrous chlorobenzene (180  $\mu$ L) was quickly dropped onto the center of the substrate and dried on a hot plate at 100 °C for 10 min. Subsequently, the PCBM:C<sub>60</sub> (8 + 12 mg mL<sup>-1</sup> in dichlorobenzene) and Bis-C<sub>60</sub> surfactant (2 mg mL<sup>-1</sup> in isopropyl alcohol) were then sequentially deposited by spin coating at 1000 rpm for 60 s and 3000 rpm for 40 s, respectively.

Finally, the device was completed with the evaporation of Ag contact electrodes (120 nm) in a high vacuum through a shadow mask. The active area of this electrode was fixed at 6 mm<sup>2</sup>. All devices were fabricated in glove box.

**Measurement and Characterization:** Solar-simulated AM 1.5 sunlight was generated using a Newport AM 1.5G irradiation (100 mW cm<sup>-2</sup>), calibrated with an ISO 17025-certified KG3-filtered silicon reference cell. The spectral mismatch factor was calculated to be less than 1%. The  $J$ - $V$  curves were recorded using a Keithley 2635 apparatus. The refractive indices ( $n$ ,  $k$ ) of perovskite were performed under a dark ambient environment by using spectroscopic ellipsometry (Woollam).

## Supporting Information

Supporting Information is available from the Wiley Online Library or from the author.

## Acknowledgements

W.E.I.S. and H.Z. contributed equally to this work. This work was supported by the University Grant Council of the University of Hong Kong (Grant Nos. 201611159194 and 201511159225), the General Research Fund (Grant Nos. 17211916 and 17204117), the Collaborative Research Fund (Grants C7045-14E) from the Research Grants Council of Hong Kong Special Administrative Region, China, ECF Project 33/2015 from Environment and Conservation Fund, and Grant CAS14601 from CAS-Croucher Funding Scheme for Joint Laboratories.

## Conflict of Interest

The authors declare no conflict of interest.

## Keywords

detailed balance, device model, efficiency loss, perovskite solar cells

Received: June 11, 2017  
Revised: September 21, 2017  
Published online: December 4, 2017

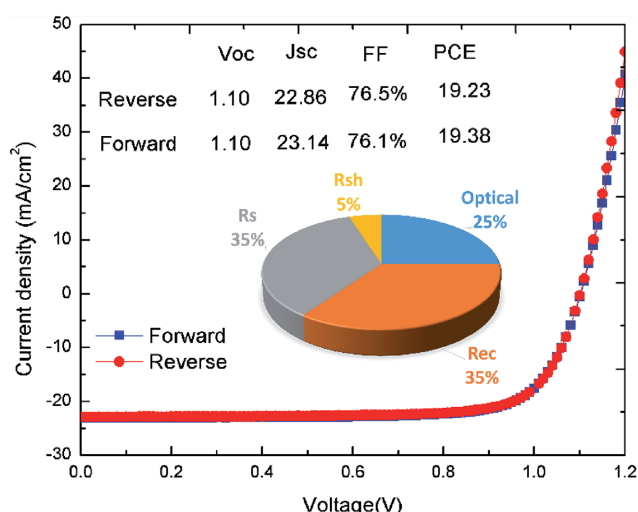


**Figure 6.** Efficiency loss of high-performance perovskite solar cells. The device structure is given as: ITO/NiO<sub>x</sub> (20 nm)/CH<sub>3</sub>NH<sub>3</sub>PbI<sub>3</sub>(Cl) (300 nm)/PCBM:C<sub>60</sub> mixture (50 nm)/Bis-C<sub>60</sub> (10 nm)/Ag (120 nm).

- [1] M. A. Green, A. Ho-Baillie, H. J. Snaith, *Nat. Photonics* **2014**, *8*, 506.
- [2] Y. C. Liu, Z. Yang, D. Cui, X. D. Ren, J. K. Sun, X. J. Liu, J. R. Zhang, Q. B. Wei, H. B. Fan, F. Y. Yu, X. Zhang, C. M. Zhao, S. Z. Liu, *Adv. Mater.* **2015**, *27*, 5176.
- [3] N. G. Park, *Mater. Today* **2015**, *18*, 65.
- [4] W.-J. Yin, T. Shi, Y. Yan, *Appl. Phys. Lett.* **2014**, *104*, 063903.
- [5] C. Wehrenfennig, G. E. Eperon, M. B. Johnston, H. J. Snaith, L. M. Herz, *Adv. Mater.* **2014**, *26*, 1584.
- [6] C. La-o-vorakiat, T. Salim, J. Kadro, M.-T. Khuc, R. Haselsberger, L. Cheng, H. Xia, G. G. Gurzadyan, H. Su, Y. M. Lam, R. A. Marcus, M.-E. Michel-Beyerle, E. E. M. Chia, *Nat. Commun.* **2015**, *6*, 7903.

- [7] S. D. Stranks, G. E. Eperon, G. Grancini, C. Menelaou, M. J. P. Alcocer, T. Leijtens, L. M. Herz, A. Petrozza, H. J. Snaith, *Science* **2013**, 342, 341.
- [8] G. C. Xing, N. Mathews, S. Y. Sun, S. S. Lim, Y. M. Lam, M. Gratzel, S. Mhaisalkar, T. C. Sum, *Science* **2013**, 342, 344.
- [9] D. Shi, V. Adinolfi, R. Comin, M. J. Yuan, E. Alarousu, A. Buin, Y. Chen, S. Hoogland, A. Rothenberger, K. Katsiev, Y. Losovyj, X. Zhang, P. A. Dowben, O. F. Mohammed, E. H. Sargent, O. M. Bakr, *Science* **2015**, 347, 519.
- [10] G. C. Xing, N. Mathews, S. S. Lim, N. Yantara, X. F. Liu, D. Sabba, M. Gratzel, S. Mhaisalkar, T. C. Sum, *Nat. Mater.* **2014**, 13, 476.
- [11] B. Yang, O. Dyck, J. Poplawsky, J. Keum, A. Poretzky, S. Das, I. Ivanov, C. Rouleau, G. Duscher, D. Geoghegan, K. Xiao, *J. Am. Chem. Soc.* **2015**, 137, 9210.
- [12] a) H. Zhang, J. Cheng, D. Li, F. Lin, J. Mao, C. Liang, A. K. Y. Jen, M. Grätzel, W. C. H. Choy, *Adv. Mater.* **2017**, 29, 1604695; b) H. Zhang, D. Li, J. Cheng, F. Lin, J. Mao, A. K. Y. Jen, M. Gratzel, W. C. H. Choy, *J. Mater. Chem. A* **2017**, 5, 3599; c) J. Mao, W. E. I. Sha, H. Zhang, X. Ren, J. Zhuang, V. A. L. Roy, K. S. Wong, W. C. H. Choy, *Adv. Funct. Mater.* **2017**, 27, 1606525.
- [13] M. Z. Liu, M. B. Johnston, H. J. Snaith, *Nature* **2013**, 501, 395.
- [14] H. Zhang, J. Cheng, F. Lin, H. He, J. Mao, K. S. Wong, A. K. Y. Jen, W. C. H. Choy, *ACS Nano* **2016**, 10, 1503.
- [15] J. Burschka, N. Pellet, S. J. Moon, R. Humphry-Baker, P. Gao, M. K. Nazeeruddin, M. Gratzel, *Nature* **2013**, 499, 316.
- [16] M. Yang, Z. Li, M. O. Reese, O. G. Reid, D. H. Kim, S. Siol, T. R. Klein, Y. Yan, J. J. Berry, M. F. A. M. van Hest, K. Zhu, *Nat. Energy* **2017**, 2, 17038.
- [17] A. Mei, X. Li, L. Liu, Z. Ku, T. Liu, Y. Rong, M. Xu, M. Hu, J. Chen, Y. Yang, M. Grätzel, H. Han, *Science* **2014**, 345, 295.
- [18] M. Saliba, T. Matsui, K. Domanski, J.-Y. Seo, A. Ummadisingu, S. M. Zakeeruddin, J.-P. Correa-Baena, W. R. Tress, A. Abate, A. Hagfeldt, M. Grätzel, *Science* **2016**, 354, 206.
- [19] K. Wang, Y. Shi, B. Li, L. Zhao, W. Wang, X. Wang, X. Bai, S. Wang, C. Hao, T. Ma, *Adv. Mater.* **2016**, 28, 1891.
- [20] H. Zhang, J. Mao, H. He, D. Zhang, H. L. Zhu, F. Xie, K. S. Wong, M. Grätzel, W. C. H. Choy, *Adv. Energy Mater.* **2015**, 5, 1501354.
- [21] S. Wang, Y. Jiang, E. J. Juarez-Perez, L. K. Ono, Y. Qi, *Nat. Energy* **2016**, 2, 16195.
- [22] W. S. Yang, J. H. Noh, N. J. Jeon, Y. C. Kim, S. Ryu, J. Seo, S. I. Seok, *Science* **2015**, 348, 1234.
- [23] W. S. Yang, B.-W. Park, E. H. Jung, N. J. Jeon, Y. C. Kim, D. U. Lee, S. S. Shin, J. Seo, E. K. Kim, J. H. Noh, S. I. Seok, *Science* **2017**, 356, 1376.
- [24] S. Selberherr, *Analysis and Simulation of Semiconductor Devices*, Springer, Vienna **1984**.
- [25] T. S. Sherkar, C. Momblona, L. Gil-Escrig, H. J. Bolink, L. J. A. Koster, *Adv. Energy Mater.* **2017**, 7, 1602432.
- [26] A. Gaur, P. Kumar, *Prog. Photovoltaics* **2014**, 22, 937.
- [27] E. J. Juarez-Perez, M. Wußler, F. Fabregat-Santiago, K. Lakus-Wollny, E. Mankel, T. Mayer, W. Jaegermann, I. Mora-Sero, *J. Phys. Chem. Lett.* **2014**, 5, 680.
- [28] W. E. I. Sha, X. G. Ren, L. Z. Chen, W. C. H. Choy, *Appl. Phys. Lett.* **2015**, 106, 221104.
- [29] W. Shockley, H. J. Queisser, *J. Appl. Phys.* **1961**, 32, 510.
- [30] X. Ren, Z. Wang, W. E. I. Sha, W. C. H. Choy, *ACS Photonics* **2017**, 4, 934.
- [31] W. E. I. Sha, W. C. H. Choy, W. C. Chew, *Opt. Express* **2010**, 18, 5993.
- [32] Y. Yamada, T. Nakamura, M. Endo, A. Wakamiya, Y. Kanemitsu, *J. Am. Chem. Soc.* **2014**, 136, 11610.
- [33] G. J. A. H. Wetzelaer, M. Scheepers, A. M. Sempere, C. Momblona, J. Avila, H. J. Bolink, *Adv. Mater.* **2015**, 27, 1837.
- [34] W. H. Press, S. A. Teukolsky, W. T. Vetterling, B. P. Flannery, *Numerical Recipes: The Art of Scientific Computing*, Cambridge University Press, New York **2007**.
- [35] F. X. Xie, D. Zhang, H. Su, X. Ren, K. S. Wong, M. Grätzel, W. C. H. Choy, *ACS Nano* **2015**, 9, 639.
- [36] C. Bi, Q. Wang, Y. Shao, Y. Yuan, Z. Xiao, J. Huang, *Nat. Commun.* **2015**, 6, 7747.
- [37] Y. Shao, Z. Xiao, C. Bi, Y. Yuan, J. Huang, *Nat. Commun.* **2014**, 5, 5784.
- [38] F. Jiang, W. C. H. Choy, X. Li, D. Zhang, J. Cheng, *Adv. Mater.* **2015**, 27, 2930.